Published in final edited form as:

IEEE Trans Biomed Eng. 2017 November ; 64(11): 2682–2694. doi:10.1109/TBME.2017.2658439.

Terahertz Imaging of Cutaneous Edema: Correlation with Magnetic Resonance Imaging in Burn Wounds

Neha Bajwa,
UCLA Dept. of Bioengineering and the UCLA Center for Advanced Surgical and Interventional Technology (CASIT), Los Angeles, CA 90095 USA

Shijun Sung [Member, IEEE],
UCLA Dept. of Electrical Engineering, Los Angeles, CA 90095.

Daniel B. Ennis,
UCLA Dept. of Radiological Sciences.

Michael C. Fishbein,
UCLA Dept. of Pathology.

Bryan Nowroozi,
UCLA Dept. of Bioengineering and the UCLA Center for Advanced Surgical and Interventional Technology (CASIT), Los Angeles, CA 90095 USA

Dan Ruan,
UCLA Dept. of Radiation Oncology.

Ashkan Maccabi,
UCLA Dept. of Electrical Engineering, Los Angeles, CA 90095.

Jeffry Alger,
UCLA Dept. of Neurology.

Maie A. St. John,
UCLA Dept., of Head and Neck Surgery.

Warren S. Grundfest [Member, IEEE], and
UCLA Dept. of Bioengineering and the UCLA Center for Advanced Surgical and Interventional Technology (CASIT), Los Angeles, CA 90095 USA

UCLA Dept. of Electrical Engineering, Los Angeles, CA 90095.

Zachary D. Taylor [Member, IEEE]
UCLA Dept. of Bioengineering and the UCLA Center for Advanced Surgical and Interventional Technology (CASIT), Los Angeles, CA 90095 USA

UCLA Dept. of Electrical Engineering, Los Angeles, CA 90095.

Abstract

(phone: 510-396-8096; fax: 310-206-2105; nbajwa1@gmail.com).

Objective—*In vivo* visualization and quantification of edema, or 'tissue swelling' following injury, remains a clinical challenge. Herein, we investigate the ability of reflective terahertz (THz) imaging to track changes in tissue water content (TWC) – the direct indicator of edema-by comparison to depth-resolved magnetic resonance imaging (MRI) in a burn-induced model of edema.

Methods—A partial thickness and full thickness burn were induced in an *in vivo* rat model to elicit unique TWC perturbations corresponding to burn severity. Concomitant THz surface maps and MRI images of both burn models were acquired with a previously reported THz imaging system and T_2-weighted MRI, respectively, over 270 min. Reflectivity was analyzed for the burn contact area in THz images, while proton density (i.e. mobile TWC) was analyzed for the same region at incrementally increasing tissue depths in companion, transverse MRI images. A normalized cross-correlation of THz and depth-dependent MRI measurements was performed as a function of time in histologically verified burn wounds.

Results—For both burn types, strong positive correlations were evident between THz reflectivity and MRI data analyzed at greater tissue depths (>258 μm). MRI and THz results also revealed biphasic trends consistent with burn edema pathogenesis.

Conclusion—This work offers the first *in vivo* correlative assessment of mobile TWC-based contrast and the sensing depth of THz imaging.

Significance—The ability to implement THz imaging immediately following injury, combined with TWC sensing capabilities that compare to MRI, further support THz sensing as an emerging tool to track fluid in tissue.

Keywords

burns; edema; medical imaging; MRI; terahertz (THz); tissue water content

I. INTRODUCTION

Maintenance of tissue fluid balance is critical for normal tissue structure and function. In the case of a tissue injury, regardless of its etiology (i.e. thermal, mechanical, toxic, or ischemic), an imbalance in interstitial fluid can occur. Resultant cell swelling and extracellular fluid accumulation in the tissue is clinically expressed as edema. Edema has important clinical consequences, including increased hydrostatic pressure within the interstitial space that 1) affects tissue function and electrical stability and 2) exacerbates the extent of tissue necrosis by microvascular occlusion [1], [2]. Edema is, therefore, an important diagnostic target for assessing the extent and severity of tissue viability *in vivo.*

The most common method for evaluating edema is by clinical examination, during which tissue swelling and turgor are routinely examined [3]. This technique, however, requires considerable clinical expertise and is very difficult to assess, if possible, when deeper tissues are involved. Adjunctive methods include water displacement volumetry that can determine the extent of edema but not its distribution in tissue [4]. The indicator-dilution technique provides a direct measurement of tissue water content (TWC) and is the current standard for assessing the distribution of body fluids. It is, however, an invasive method that requires

blood sampling. Given the need for a clinically acceptable, non-invasive, and accurate technique for detecting edema, *imaging* TWC could provide useful spatiotemporal diagnostic and prognostic information.

Early evidence suggests that visualization of TWC changes in superficial tissues may be possible with reflective terahertz (THz) imaging [5]–[7]. The THz band refers to non-ionizing electromagnetic waves in the 100 GHz to 10 THz frequency range [5], [6]. Reflection imaging of biological tissue at THz wavelengths has shown high contrast in rapidly and efficiently distinguishing abnormal tissue from healthy tissue in cornea and in skin injuries [7]–[10]. Reflective THz imaging is unique in that it: I) offers distinct advantages over earlier transmission-based systems for *in vivo* applications due to the high THz absorption in tissue [6], [8], [11]; II) probes the dielectric properties of tissues using simple optical components [5], [6], [12], [13]; and III) is minimally perturbed by surface characteristics like hair and tissue surface roughness [5], [14]. Unlike depth-resolved images of tissue acquired with magnetic resonance imaging (MRI), THz images of tissue are 2-dimensional (2D) reflection maps representing an aggregate tissue property. Because water constitutes ~70% of the weight of soft tissue, and the THz frequency dielectric constant of water is significantly higher than that of non-water constituents, the aggregate reflected signal observed with *in vivo* THz imaging is interpreted as TWC [15], [16]. However, liquid water displays broad absorption bands rather than narrow absorption signatures in the THz band. Consequently, this observation does not identify TWC as the primary source of contrast in THz imaging. Therefore a companion imaging modality is currently needed to interpret contrast in THz tissue data [5].

A recent study on THz contrast has proposed using MRI to verify the contributions of TWC to THz imaging of superficial tissues [17]. Despite its limited access and associated costs, MRI resolves depth information and provides comprehensive, layer-specific anatomical and physiological data on TWC in a single setting. Among the multitude of sequences available, T_2-weighted (T_2w) MRI has previously been used to visualize the hydration state of skin *in vivo* [18]–[20], [20]. In T_2w images, skin layers filled with water appear bright and tissues with high fat content appear dark. Tissue contrast in T_2w MRI is primarily determined by differences in the transverse component of proton relaxation time (T_2), where longer T_2 relaxation times are associated with protons that are part of mobile water molecules and shorter T_2 times are associated with lipid-rich environments. Relative proton density - the fraction of mobile water protons available in the tissue - can be directly calculated from the T_2 relaxation time in T_2w images [21]; measured proton density is associated with water and no other macromolecules (i.e. lipids) when T_2w MRI imaging is used. In fact, relative proton density has been used to distinguish protein-bound water from “free” water (i.e. effusion or edema) in superficial tissues that have also been explored with THz imaging. These tissues include uninjured and diseased skin *in vivo* [20], [22], [23] as well as wounds of increasing severity (superficial, superficial partial, deep partial, and full thickness) *ex vivo* [16]. Among wound models, *in vivo* burn injuries are characterized by the biggest inflammatory reaction and result in substantial and rapid edema formation [24]–[26].

Herein, we seek to investigate the potential of THz imaging for edema assessment by correlating THz frequency tissue reflectivity measurements with relative proton density

measurements captured by T_2w MRI in burn-induced edema models. It is important to note that MRI is only used here for pre-clinical research purposes, as its cost and limited portability make it inappropriate for TWC characterization in patients, especially critical patients. Burn wounds in rats are known to severely and acutely perturb TWC and, thus, were selected as the model for this correlative study [27]–[31]. A partial thickness burn and a full thickness burn were induced *in vivo* to the abdominal skin of rats using an established contact wound protocol that exhibits markedly different TWC perturbations corresponding to burn severity [10], [32]. Partial thickness, or 2nd degree, burns involve the epidermis and dermis to reticular dermis skin layer [33], [34]. Full thickness, or 3rd degree, burns involve the whole thickness of the skin and possibly subcutaneous tissue [33].

Concomitant THz and MRI images of both burn models were acquired with a previously reported reflective THz system and 7T MRI prior to thermal insult, 90 min, 210 min, and 270 min following burn induction [6], [10], [16]. Previous work in THz wound imaging has shown that partial thickness and full thickness burns produce pronounced and distinct spatiotemporal changes in THz image contrast. Therefore, similar to THz imaging, we hypothesized that MRI TWC-based contrast would: I) exhibit unique signal characteristics for each wound model; and II) agree with trends observed in the companion THz burn imagery [6], [10], [35].

Following histological assessment of burn severity in each wound model, a one-to-multiple cross-correlation across time was performed between THz and depth-dependent MRI imaging, respectively; at all time points, a single reflectivity measurement across the burn region in the THz image was compared to relative proton density measurements performed at multiple burn depths in the companion MRI image to: I) investigate mobile TWC (i.e. edema) as the underlying biophysical driver of observed changes in THz reflectivity and II) quantify, for the first time *in vivo,* the tissue depths at which THz imaging can potentially probe edema.

II. Materials And Methods

A. Injury-Induced Cutaneous Edema

All experiments were approved by the Institutional Animal Care and Use Committee (IACUC). Two male Sprague Dawley rats weighing 180–200g (Harlan laboratories, Hayward, CA) were used as preclinical models to investigate the effects of burn-induced edema on reflective THz imaging contrast. While pigs are a more appropriate genomic model of human skin, THz imaging in bulk tissue is insensitive to molecular-based mechanisms [36]. Rats are also widely available, convenient in size, and tractable in nature, lending them as an attractive model [32]. Finally, there are few known differences in edema physiology between rats and other candidate animal models.

Surgical preparation of the rats began with administration of extrinsic intradermal fiducial markers to allow for image registration between the THz images, visible images, and histology. 72 h prior to burn induction, each rat was anesthetized using isoflurane (4% and 1% for induction and maintenance, respectively), the skin from the abdomen was shaved to expose a 5 cm × 5 cm area of bare skin, and three tattoos were applied to the abdomen;

intradermal injections of non-metallic green ink were administered via a sterile 28G needle to form the apices of a right triangle. Once tattooed, both subjects were awoken and allowed to recover for 72hr.

B. THz and MRI Imaging Systems

A 7T small bore MRI scanner (Bruker Biospin, Switzerland) was used to acquire MR imagery of *in vivo* burns [16]. To obtain high-resolution images a 160 mm gradient was used to achieve a pixel size of 86 microns in depth in combination with a small surface radiofrequency coil (3 cm in diameter) to improve the signal-to-noise ratio (SNR). High-resolution T_2w multislice multiecho (MSME) MR images of abdominal skin prior to and following burn induction were obtained by varying T_e (T_r = 500 ms, eight TE values including 14, 28, 42, 56, 70, 84, 98, and 112 ms) within a 44 × 11 mm^2 field of view (FOV) and a slice thickness of 2 mm, corresponding to a voxel dimension of 172 × 86 × 2000 μm^3. A total stack of six axially oriented MRI slices required an image acquisition time of ~40 min. The aforementioned protocol has previously been used to acquire spatially resolved imagery of *ex vivo* skin burns with high contrast and SNR [16].

A reflective THz imaging system was used to acquire THz images of uninjured skin and burn tissue [6], [8], [10]. The THz system operates in reflection mode at a center frequency of 0.525 THz with ~125 GHz bandwidth. The effective center frequency and bandwidth of the system are constrained by the THz source's power spectral density and the detector's spectral responsivity. As reported in our previous *in vivo* THz imaging work, this bandwidth is sufficient to overcome speckle and is sensitive to changes in tissue water content with good spatial resolution [37]. The system consists of a photoconductive switch based THz emitter, Schottky diode detector, and a novel gated receiver for high SNR, high dynamic range measurements of THz power. The Schottky diode detector is mounted in a 0.381 × 0.1905 mm rectangular waveguide (WR1.5) to limit the system detection to the 400 GHz – 700 GHz band. These spectral parameters are chosen to balance TWC sensitivity and sufficient spatial resolution, while mitigating clutter in the acquired image [6]. The THz beam is handled by quasi-optical imaging system that focuses the radiation to a 1 mm^2 diameter spot at a 36 mm standoff distance. THz imagery was generated by raster scanning the imaging subject beneath the fixed, focused THz beam at a 1 ms per-pixel integration time. An image with a 60 mm × 60 mm FOV required a scanning time of ~10 min using a 0.5 mm step size.

On the day of the burn study, visible and THz images of the uninjured, tattooed abdominal skin of anesthetized rats in supine position were captured with an SLR camera and the THz imaging system. In comparison, control scans of the animal in prone position were acquired using a T_2w MSME sequence with the 7T animal instrument. A 12 μm thick optical Mylar window (~3.1 cm in diameter), transparent to THz illumination, was lowered onto the abdominal skin during THz imaging to flatten the imaging plane and minimize effects from non-uniform surface contours.

Before MRI imaging, the Mylar window was removed and two 0.75 cm MRI fiducial markers (Radiance filled Ortho-SPOT Packets, Beekley Medical, Bristol, Connecticut) were positioned superior and inferior to the designated burn induction area and a visible image

was acquired. The rat was then placed on the surface coil in prone position for MRI scanning of the uninjured skin; this positioning of the coil on the abdominal skin increased the SNR.

Upon completion of the control scans, a full thickness and partial thickness burn were induced on the rat abdomens. A 2 mm × 19 mm rectangular brass brand was secured to a thermocouple (OMEGA, Stamford, Connecticut) to accurately monitor the absolute temperature of the brand. The brand was heated to 200°C and 130°C using a hot plate, positioned between the fiducial markers using a high-precision manual z-stage, and applied to the abdomen with a constant pressure for 10s to induce a full thickness and partial thickness burn, respectively [10], [16]. Each rat received one burn to minimize the total burned body surface area, thus reducing effects of shock on the physiologic wound response.

Visible and THz imaging of a burn region covered a 60 mm × 60 mm FOV. THz images only include tissue under the Mylar window, and this measures 11.4 cm^2. MRI covered a registered volume of 44 mm × 11 mm × 92 mm. Parallel THz and MRI imagery were acquired continuously over a 5 h period. The rats were then returned to the vivarium and euthanized 3 days following burn induction because the final status of a burn wound typically manifests 72 h following thermal insult [26].

C. THz and MRI Image Analysis

It is important to clarify the kind and spatial dimension of information captured in a THz image of tissue versus that in a MRI image of the same specimen. THz imaging furnishes a 2D *surface* reflection map of tissue that arises from the column integrated electromagnetic properties of the tissue down to a depth limited by absorption, system SNR, etc. Consider the recursive field reflection coefficient in equation (1) [9], [38].

$$\Gamma_i = \frac{\rho_i + \Gamma_{i+1} e^{-j2\delta_i}}{1 + \rho_i \Gamma_{i+1} e^{-j2\delta_i}}, \qquad \Gamma_{N+1} = \rho_{N+1} \quad (1)$$

This equation describes the field reflectivity of a stack of N homogenous, isotropic layers with uniform thickness sandwiched between two half spaces. Γ_i is the field reflectivity of the stack from layer i to N, ρ_i is the field reflectivity from layer i-1 to layer i and δ_i is the complex path length of layer i. In a skin model, Γ_i, ρ_i, δ_i are all functions of the layer thickness and the water content at a particular layer. In the limit of optically thin layers, the aggregate reflectivity of skin (which displays a water content gradient) can be simulated by increasing the number of layers until the forward traveling incident radiation has been attenuated to some appreciably small level and then terminating the stack with a half space whose electromagnetic properties are equal to the final stack layer. Using the established formalism, we write the field reflectivity of the skin as Γ_1.

For this study we assume that imaging contrast is strongly dependent on tissue water content, and thus the reflectivity of skin is a function of transverse dimension (x,y) and the

tissue water content is a function of observation time (tm): $\Gamma_1 \rightarrow \Gamma_1(t_m, x, y)$. The system utilizes a 0-bias rectifier and thus the system pixel value is a function of the THz reflectivity of the pixel position:

$$R(t_m, x, y) = \left|\Gamma_1(t_m, x, y)\right|^2 \quad (2)$$

The recursive relation equation (1) continually references the electromagnetics properties of adjacent layers and thus equation (2) can be thought of as a column integrated (weighted average) reflectivity with the depth dependent weighting described by the term $e^{-j2\delta_i}$

Thus, similar to its companion visible image, a THz image is represented only in the horizontal (x) and vertical (y) dimensions and, therefore, does not provide reflectivity resolved in the depth (d) dimension (Fig. 1A). THz image sets are displayed in a standard false color map where black-red-yellow-white denotes increasing reflectivity. For all time-series THz burn images, a white linear contour measuring 5 mm was drawn to transversely segment the burn contact tissue along the x-dimension. Pixel-by-pixel reflectivity values of the white contour were normalized to the maximum THz reflectivity acquired from an aluminum calibration target (i.e. ideal reflector) and zero THz reflectivity measured in the absence of a reflecting target (i.e. air). The calibrating reflector was positioned in the same manner and stand-off distance as abdominal skin during the initial THz system scans. Using the mean value theorem, the mean reflectivity of the contour at time t_m along the length of the contour, x, is expressed as

$$R(t_m) = \frac{1}{\Delta x}\int_{\Delta x} R(t_m, x)dx \quad (3)$$

$R(t_m, x)$ was calculated at all time points for both burn wound models. Using this analysis of THz imagery, a *single* profile of mean reflectivity associated with the burn image feature (i.e. white linear contour) was plotted as a function of *time* for both a partial thickness and full thickness burn wound model.

While the companion MRI scan is similarly 2D (Fig. 1B), this image provides the spatial distribution of TWC in burn tissue along the x-dimension and across multiple skin layers (i.e. d-dimension). Specifically, the x-dimension of every T_2w and T_2-mapping image pair spatially maps to the length of the white linear contour drawn in its companion THz image. Mapping between MRI, visible, and THz imagery was achieved by capturing contiguous MRI slices of known thickness (2 mm) along the y-dimension of the burn, measured to be ~20 mm, that include the MRI fiducial markers. MRI images are displayed in a gray-scale color map where black-grey-white indicates increasing intensity and T_2 relaxation time for T_2W and T_2-mapping images, respectively. The MRI signal, S, for a T_2W image is:

$$S = k \cdot N\exp\left(-\frac{T_E}{T_2}\right) \quad (4)$$

where k is a function of the instrument's receiver gain, N is proportional to the mobile proton density, T_2 is the transverse MR relaxation time, and T_E is the echo time.

Parametric analyses were performed on T_2-mapping MRI slices at T_e= 28 ms. Those MRI slices with the greatest observable contrast in the dermal layer of the burn were selected for image analysis at each time point. These slices mostly reside in the center of the wound, and therefore did not capture the fiducial markers positioned at the extremes of the MRI slice stacks. To analyze mean T_2 relaxation time and mean relative proton density (i.e. mobile TWC) as a function of depth in each T_2-mapping image, a white contour, measuring 5 mm in length, was drawn along the x-dimension of the burn contact area. The same contour was superimposed at incrementally increasing depths (~86 μm) in the dermis, measuring ~700 μm in thickness.

For all time points (t=0 min, 90 min, 210 min, and 270 min), the mean T_2 time and the associated standard deviation was calculated using ImageJ (NIH, Bethesda, MD) by fitting to relation to equation (4) the signal intensity S from the contour at every depth in T_2-mapping images. Note that S is a function of the instrument's receiver gain, k, which is optimized for each longitudinal time point. Consequently, N of the burn tissue was normalized to that of the previously described MRI fiducial marker to obtain comparable N values across all time points in the study. Mean proton density at time t_m and depth d_n is expressed as

$$N(t_m, d_n) = \frac{1}{\Delta x}\int_{\Delta x} N(t_m, d_n, x)dx \quad (5)$$

Using this analysis of MRI imagery, *multiple* profiles of mean T_2 time and relative proton density associated with the image feature (i.e. white linear contour) were plotted as a function of *time* and *depth* for both burn wound models.

Collectively, this THz and MRI image analysis demonstrates there is a one-to-multiple relationship between THz imaging and MRI data, respectively, at each time point; for both burn types, THz imaging results are plotted as a single temporal profile, whereas MRI imaging results are plotted as unique temporal profiles for each tissue depth. Because only relative proton density is a direct measure of mobile TWC, a one-to-many correlation across time was required between THz reflectivity of the burn region and relative proton density measurements acquired by MRI at specific tissue depths in the same tissue. Using this type of correlation, we can not only investigate how well THz reflectivity correlates with TWC-based MRI measurements, but also determine at which MRI depths in the tissue these correlations are strongest. This analysis addresses the core aims of the study: 1) to

investigate TWC-based contrast of THz imaging and 2) determine tissue depths at which THz imaging can probe TWC.

D. Normalized Cross-Correlation

Normalized cross-correlation is a method that can be used to compare reflectivity and depth-dependent relative proton density of images acquired with THz imaging and MRI, respectively, by first normalizing these measurements and then calculating the displacement of one relative to the other. This is also known as a sliding dot product. Vectors of time dependent variables used in the normalized cross-correlation are defined as follows;

$$\overrightarrow{N}(d_n) = \begin{bmatrix} N(t_1, d_n) & N(t_2, d_n) & N(t_3, d_n) \end{bmatrix} \quad (6)$$

$$\overrightarrow{R}_{THZ} = \begin{bmatrix} R(t_1) & R(t_2) & R(t_3) \end{bmatrix} \quad (7)$$

The cross correlation coefficient of the THz time series with the depth dependent MRI relative proton density series is written as the inner product

$$\rho(d_n) = \left\langle \frac{\overrightarrow{N}(d_n) - mean\left(\overrightarrow{N}(d_n)\right)}{\left\|\overrightarrow{N}(d_n) - mean\left(\overrightarrow{N}(d_n)\right)\right\|}, \frac{\overrightarrow{R}_{THz} - mean\left(\overrightarrow{R}_{THz}\right)}{\left\|\overrightarrow{R}_{THz} - mean\left(\overrightarrow{R}_{THz}\right)\right\|} \right\rangle \quad (8)$$

where the mean and magnitude of a vector $\overrightarrow{v}$ in $\mathbb{R}^M$ is:

$$mean(\overrightarrow{v}) = \frac{1}{M}\sum_{m=1}^{M} v_m \quad (9)$$

$$\|\overrightarrow{v}\|^2 = \sqrt{\sum_{m=1}^{M} |v_m|^2} \quad (10)$$

The inner product of the two vectors, $\overrightarrow{u}$ and $\overrightarrow{v}$, in $\mathbb{R}^M$ is:

$$\langle \overrightarrow{u}, \overrightarrow{v} \rangle = \sum_{m=1}^{M} u_m v_m \quad (11)$$

The result is a temporal correlation coefficient (p) between THz reflectivity across the burn and relative proton density at each MRI burn depth for both a partial thickness and full thickness burn wound.

E. Histological Assessment

A blind histological analysis of burn tissue harvested at 72 h post injury was compared to visible imagery to assign burn severity. Histological features in burn wounds are known to manifest by 72hr following thermal insult, and therefore this endpoint was used to harvest tissue and histologically determine burn severity (i.e. partial thickness and full thickness) (Fig. 2). Three regions of the burn wound (i.e. left, center, and right) were harvested, transferred to 10% formalin solution, and submitted for histopathological evaluation. All tissue samples were sectioned orthogonal to the major axis of the burn and some contained an intradermally injected tattoo marker for orientation of the tissue specimen. Six histological slices of 5|im thickness were acquired from each tissue block, stained with hematoxylin and eosin, and analyzed to determine burn severity. Histology sections included both burned and healthy areas, providing a control area consisting of unburned tissue to which the burned area was compared. A blind investigation of depth of injury was used to confirm that the 130°C and 200°C wound were a partial thickness and full thickness burn, respectively. Complete epidermal necrosis, muscle necrosis, collagen discoloration, and occluded vessels were used to characterize a full thickness wound. In regards to depth of injury, these histological features extend into the dermis and subcutaneous layer. In contrast, patent vessels as well as intact skin and muscle tissue that did not exhibit signs of cellular damage were used to classify a partial thickness wound [10].

III. Results

Parallel THz and MRI time-series imagery of a partial thickness bum and full thickness bum induced in the abdominal skin of anesthetized rats were acquired over a 5hr period (Fig. 3). This time window was selected based on previous observations of apparent morphological changes in the FOV and motivated by the evolution of the wound response following acute injury [39]. During THz imaging, burn wounds were imaged under a thin (12 μm) film Mylar window to eliminate confounding effects from non-uniform surface contours (Fig. 3A). Solid red arrows and dotted red arrows in MRI images of Fig. 3B denote the location of the burn contact area and resultant edema formation in the dermis, respectively. Visual inspection of the time-series MRI images shows the positions of these arrows are not at their original position. This shift in position is neither arbitrary nor relevant to tissue swelling, but instead due to the difficulty in repositioning the animal after transferring the subject between the MRI scanner and THz imager at each time point. Despite the red indicators not being spatially registered, the burn contact area and resultant edema are successfully captured in the FOV of MRI images for both subjects at all time points.

Temporal profiles of normalized THz reflectivity were generated for the burn contact site in each wound model (Fig. 4). In comparison, multiple temporal profiles of mean T_2 time and relative proton density were generated for specific tissue depths associated with the same burn contact region in spatially mapped MRI image sets (Fig. 4).

THz images of the rat abdomen prior to inducing a full thickness and partial thickness burn (Fig. 3A) display mostly uniform THz reflectivity across the FOV. Companion mean T_2 times of the epidermis (T_2=34±5 ms), dermis (T_2=26±7 ms), and hypodermis (T_2=57±8 ms)

are consistent with previously published *in vivo* MRI values for skin (t=0 min in Fig. 3B) [20], [22].

Following thermal insult (t=90 min), THz reflectivity across the burn region and T_2 time and relative proton density of burn tissue at tissue depths > 258 μm rise and fall together with a biphasic trend. As originally hypothesized, the evolution of THz reflectivity and MRI tissue measurements is not identical for each wound severity. For a full thickness wound immediately following burn induction, THz imaging captures a drop in THz reflectivity in the wound contact area (Fig. 4A–B) while MRI detects an increase in relative proton density (i.e. mobile TWC) in the same burn region with respect to uninjured skin (t=0 min). This increase in relative proton density is evident across varying depths – between 172 and 688 μm – in the dermis of the burn tissue (Fig. 4A).

By comparison, a partial thickness wound is characterized by an increase in both THz reflectivity and relative proton density in the burn contact area for depths > 258 μm immediately following thermal injury (Fig. 4C). These measurements are also greater in magnitude than those in a full thickness wound. For example, at a depth of 516 μm, relative proton density (Fig. 4C) and T_2 time (Fig. 4D) for the same region of a partial thickness wound at t=90 min compared to that of uninjured skin are 3.6% and 7% greater, respectively. The corresponding THz reflectivity for a partial thickness burn is calculated to be 7% greater than that of uninjured skin. In contrast, reflectivity and MRI differences between burn tissue and uninjured tissue are not as substantial in a full thickness wound at t=90 min. MRI and THz parameters associated with the burn contact area both peak at t=210 min and visibly decline at t=270 min in each of the two burn severity models. For a depth of 516 μm at t=210 min the THz reflectivity, T_2 time, and relative proton density of a partial thickness wound are 20%, 45%, and 7% greater, respectively, than values in uninjured tissue. In contrast, all mean THz and MRI measurements at their temporal peak for a full thickness wound are lower in magnitude; for the corresponding dermal depth at 210 min the THz reflectivity, T_2 time, and relative proton density are 1%, 15% and 5% greater, respectively, in a full thickness wound compared to uninjured skin. Finally, a concurrent decline in mean THz reflectivity, T_2 time, and relative proton density becomes visible in both burn types by t=270 min (Fig. 4).

IV. Discussion

Because edema is a generic component of the tissue injury response, it has become an important diagnostic indicator of tissue viability. In the past, edema could not be used as a diagnostic target, because the extent and distribution of cellular edema was difficult to qualitatively or quantitatively assess under the microscope; even with increases as large as 100% in cell volume, the cellular diameter increases by only 26% [40].

Although electron microscopy may reveal the presence of edema features including membrane blebbing, detachment of actin filaments, and swelling of the endoplasmic reticulum, this technique is not suitable for assessing the regional extent and distribution of edema, especially in patients. *In vivo* imaging methods, such as MRI, have augmented this but are still financially and practically incompatible with a range of edema-related

applications. Moreover, the lengthy acquisition times required to obtain an image render these technologies unsuitable for detecting or monitoring the acute, and often rapidly developing onset of edema. Early visualization of fluid shifts, therefore, specifically calls for TWC imaging capabilities on the order of minutes for a FoV that spans the injured area.

Rapid THz imaging systems have previously been used to generate pathology-specific contrast in burn wounds, cancer tissue, and cornea *in vivo* [8], [10], [15], [17], [35], [37], [38]. Although novel, these results, do not I) confirm mobile TWC (i.e. edema) as the dominant contrast mechanism of THz imaging or II) quantify tissue depths at which THz imaging can potentially probe TWC. Such a validation study requires correlating THz imaging to a modality that not only relies on TWC to generate image contrast, but also one that affords cross-sectional images of tissue in the depth dimension. MRI is a method for both evaluating and spatially localizing TWC *in vivo.* Specifically, T_2w MRI furnishes depth-dependent parameters – T_2 relaxation times and relative proton density – that are both sensitive to the amount and the physical state of TWC [41]; an increase in T_2 time and proton density is directly correlated with greater TWC [42]. Burns are characterized by massive shifts in TWC (i.e. edema), and, therefore, serve as an appropriate injury model to investigate TWC-based THz imaging contrast. By comparing THz imaging to T_2W MRI, we demonstrate that it is possible to use reflective THz imaging to rapidly and non-invasively track fluid shifts in an *in vivo* injury-induced edema model with excellent contrast and sensitivity. THz reflectivity measurements of the burn contact area rise and fall with companion MRI measurements acquired of the burn tissue region at greater skin depths (>258 μm) as a function of time. Moreover, the biphasic pattern and distinct magnitudes of these measurements for both burn types agree with burn edema pathogenesis commonly observed in partial thickness and full thickness wounds as well as predicted electromagnetic behavior of tissue [26].

Immediately following burn induction of a full thickness burn (t=90 min), THz imaging captures a drop in THz reflectivity in the wound contact area (Fig. 4A–B) while MRI detects an increase in relative proton density (i.e. mobile TWC) and T_2 time in the same burn region with respect to uninjured skin (t=0 min). This increase in both MRI parameters is evident across varying depths – between 172 and 688 μm – in the dermis of the burn tissue (Fig. 4A). The inconsistency between measurements acquired with both imaging modalities is not arbitrary but instead explained by burn pathophysiology and how this tissue response markedly varies in the first hour following a full thickness injury: a survey of the literature indicates burn edema pathogenesis of a full thickness wound is first characterized by an immediate, localized drop in mobile TWC due to a transient cessation of vascular perfusion [25], [26]. This response is only on the order of minutes. With respect to THz-tissue behavior, stratified media modeling of skin predicts that the THz reflectivity of a tissue system imaged at our center operating frequency (~525 GHz) decreases approximately linearly with decreasing TWC [9]. Because THz imaging (~10 min acquisition time) is performed before MRI (1 hr acquisition time), this immediate decrease in TWC for a full thickness burn is observed as a decrease in THz reflectivity; Following this initial, transient drop in TWC, a full thickness wound is known to be characterized by a subsequent increase in TWC [26]. Because an MRI image takes approximately an hour to acquire, TWC captured in these images correspond to the second phase of the full thickness burn edema

response: the increase in TW C is reflected by a greater T 2 relaxation time and relative proton density at t=90 min with respect to the pre-burn values. After t=90, THz reflectivity trends mirror those observed in companion T_2 times and proton density measurements at greater skin depths (>258 μm); both modalities visualize the same phase of the burn edema response, and therefore identical TWC. Because both THz and MRI measurements did not visualize the same TWC content at t=90 min, this time point was excluded in the normalized cross-correlation of the full thickness burn.

As expected, THz and MRI measurements for a partial thickness burn at t=90 min both increase with respect to uninjured skin because this wound type is not known to be characterized by an immediate, transient drop in TWC; a partial thickness burn wound is characterized by immediate and greater mobile TWC (i.e. pronounced arteriolar vasodilation), and, therefore, its THz and MRI imagery is expected to show greater THz reflectivity and relative proton density from the time of burn induction [25], [26].

The immediate change in reflectivity between uninjured tissue and injured tissue differs from that reported in previous studies, likely due to 1) the heterogeneity in TWC between uninjured subjects and 2) the type of burn induction technique used [15], [35]. While some THz burn studies use a scald burn method, our group induced a contact burn wound using a heated brand in rat skin [10], [37]; exposing the prepared skin to a heated brand causes immediate tissue coagulation, with a clear demarcation between viable and necrotic tissue [43]. This layer of necrotic tissue is similar to a dry eschar, which appears to block the heat conduction to the deep vascular plexus, thus resulting in small, while still observable perturbations in TWC and THz reflectivity [43]. In a scald burn, there is no necrotic layer which can function as a barrier to stop conduction. Therefore, the deep vascular plexus is damaged, resulting in large TWC perturbations, and, therefore, large changes in reflectivity between uninured and injured tissue [43]. Burn severity using a scald technique, however, is less controlled [44].

While both MRI and THz data peak at t=210 min for both burn models (Fig. 4), peak values observed in the partial thickness wound are greater than those of a full thickness wound. These findings agree with well-established reports of peak edema being greater in partial thickness burns than in full thickness burns due to a marked decrease in dermal perfusion as burn depth increases [24], [26]. The difference in the quantity of edema formation between a partial thickness and full thickness burn is based on the local capillary and interstitial changes as well as the general status of the vascular space [45]–[49]. Most of the vasculature and lymphatics are located in the dermis layer [50]–[53]. In a full thickness burn, which affects all the skin layers, the dermal lymphatics are destroyed, impairing the transport of fluid to the burn site. This effect results in decreased blood volume and blood flow to the burn tissue, which, in turn, results in less edema compared to a partial thickness burn (i.e. TWC) [25], [26], [54]. Conversely, partial thickness burns only involve the epidermis and some layers of the dermis, and, as a result, the underlying vasculature is les damaged compared to a full thickness wound. This result leads to better vascular perfusion, and therefore more edema (i.e. TWC) in partial thickness burns [25], [54]. As shown by Fig. 4, the partial thickness burn tissue is characterized by higher total water content, that is proton density sensitive [42]. A coincident increase in water binding capacity, that is T_2 sensitive,

results in greater magnitudes for T_2 time in the partial thickness wound. As expected, THz reflectivity of a tissue system of higher TWC (i.e. a partial thickness burn) is greater than that of a tissue system of lower TWC (i.e. a full thickness burn). Deeper layers of partial thickness wounds are also known to have increased edema, which is reflected by the higher mean relative proton densities that characterize MR measurements at greater depths (Fig. 4C) [26]. The concurrent decline in THz and MRI parameters in both burn severities by t=270 min (Fig. 4) is consistent with the start of the final resorption phase of the edema response [25].

In both burn models, THz reflectivity of burn tissue correlates with parallel measurements of depth-dependent relative proton density as a function of time (Fig. 5). The most important result is that the correlation between THz and MRI measurements is strong for depths greater than ~300 μm; layers of the dermis (300–600 μm) are known to experience the greatest changes in TWC following injury [26], [54]. Specifically, strong positive correlations are evident at greater depths in the dermal tissue: at 688 μm, temporal coefficients (p) computed with normalized cross-correlation are as high as 0.97 and 0.86 for a full and a partial thickness wound, respectively. Depth-dependent variation in p is also correlated between the wound severities. These results suggest that mobile TWC strongly contributes to the observed THz imaging contrast, and that THz imaging tracks movement of water at dermal tissue depths that are relevant to edema assessment [24]–[27], [55].

THz reflectivity and companion TWC measurements of the upper dermis (at 86 μm and 172 μm) are anti-correlated. These depths, however, correspond to skin layers and tissue interfaces (i.e. the dermoepidermal junction) that are not known to contribute to the edema response, and, therefore, are less clinically significant and only of scientific interest. [22]. Because MRI signal varies markedly at tissue boundaries, anti-correlations at these depths may be due to system-related constraints and not pathophysiology. Conversely, changes in signal may also be due, in part, to wave interference effects. Further THz electromagnetic modeling work is currently being performed to explore the potential thin film-like properties of these tissue layers. Similar to stratified media modeling previously published on the cornea, a detailed, layer-by-layer, model of burn tissue is required [9]. Many groups have published on the accuracy of using the double Debye model as a baseline and perturbing the relaxation time until the fit converges with the observed spectra [9], [56]–[59]. Our group proposes to use effective media theory to compute tissue dielectric properties through the use of the estimated fill factor of water to tissue. When the tissue water content is changed by thermal insult and the subsequent physiologic response, the fill factor can be modified to compute the effective dielectric function at the tissue hydration of interest. This methodology models what is thought to occur in burn wounds and serves as a good starting point when performing system design calculations for expected reflectivity, sensitivity, etc. To illustrate the variability of the skin electromagnetic properties, two candidate variation types will be explored: 1) localized TWC perturbation, where the edema occurs primarily at the epidermis/dermis interface; and 2) global variation with fixed surface hydration where the edema penetrates all the skin layers but the top surface remains intact.

From a technological standpoint, the TWC shifts that we observed with THz and MR imaging are the first to be imaged *in vivo* for both modalities. Furthermore, a comparative

analysis shows that THz imaging can offer rapid measurements on TWC for potential edema assessment and provide these measurements earlier than existing clinical and research techniques (Table 1). The time frame of edema assessment includes 1) the time when the technique can be implemented and 2) the acquisition time. Contributions from both measurements are of clinical importance for early and rapid detection of fluid shits following cutaneous injury.

Although a clinician's assessment typically requires the least amount of time to perform, the clinical manifestations of edema occur secondarily to the subcutaneous accumulation of edematous fluid and adipose tissue; visual assessment of edema is delayed by a few hours because fluid build-up -perceived clinically as an increase in tissue volume - is only visually apparent after tissue volume has doubled [60]. Water displacement methods, during which the affected area is submerged in a cylinder filled to a known level of water and the amount of water displaced by the tissue measured, are very time-consuming; two successive measurements require ~ 20–30 min, while the setup alone involves an additional 30 min [4]. This technique, therefore, is not suitable for measurement of TWC of patients in the immediate postoperative period. In comparison, histochemical evaluation of tissue biopsy samples can take on the order of days due to the preparation and processing times [61].

Among the techniques listed in Table 1, only THz and MRI imaging can be used immediately following injury. Although a powerful tool, MRI of the skin, at present, functions mainly as a research technique. The clinical utility of MRI for diagnosis of burn wounds or tissue viability based on resultant edema remains unknown, largely due to patient-related factors, including delays in self reporting, and technological constraints.; slow data acquisition times, cost, and limited access essentially preclude the use of MRI for the detection of processes such as acute inflammation or edema. For example, a T_2w MRI image measuring 44 mm × 11 mm requires ~40–60 min to acquire, while our THz imaging system acquires a larger FOV (60 mm × 60 mm) in ~10 min using limited rectilinear scanning speed. Further, improved beam scanning designs and automation techniques will allow image acquisition time limited only by SNR. Currently our pixel acquisition time is 10 ms/pixel. We anticipate an acquisition lower limit of 60 mm × 60 mm / 0.5 mm / 0.5 mm × 10 ms/pixel = 144 seconds with no degradation in per pixel SNR.

Although the spatial resolution of THz images is generally inferior to that of images generated by high-field animal MRI, the transverse resolution is on par with MRI systems. Furthermore, the high contrast and speed (with respect to T_2W MRI) of THz imaging, combined with sensing capabilities that correlate with those of TWC-based MRI, suggest that THz imaging may surpass MRI in early TWC assessment. Future efforts should facilitate the translation of THz technology for clinical use through improvements in imaging speed and optical architectures. These advancements may enable both timely and informed THz mapping of tissue edema and the extent of fluid extravasation into tissues in patients sustaining severe burn injuries, trauma, or other medical conditions leading to fluid shifts [64].

V. Conclusions

Edema, the build-up of fluid in tissue, is often an underlying cause of infection and morbidity. Quantifying and visualizing edema, however, remains a clinical challenge. We show that it is possible to non-invasively and rapidly detect fluid shifts in burn-induced edema models using reflective terahertz (THz) imaging. THz imaging of a partial thickness and full thickness burn wound induced in an *in vivo* rat model was correlated with companion T_2-weighted magnetic resonance imaging (MRI), which relies on tissue water content (TWC) to generate contrast and offers TWC measurements in the depth dimension. This study was the first *in vivo* correlative assessment to investigate TWC-based contrast mechanisms and the probing depth of THz imaging. Normalized cross-correlation was used to compare THz reflectivity across the burn contact area with proton density measurements performed along the same region as a function of depth in the tissue for spatially mapped, transverse MRI imagery. Proton density measurements associated with greater burn depths in MRI imaging more strongly correlated with reflectivity of the burn region in THz imaging. For both a partial thickness and full thickness wound, the time course and magnitude of THz reflectivity and MRI measurements reflected known trends observed in burn edema pathogenesis. These combined results suggest THz imaging could enable earlier tissue viability assessment and treatment in patients sustaining severe burns, trauma, or other conditions leading to profound tissue edema.

Acknowledgements

The authors would like to thank Dr. Andrew Frew at the Ahmanson-Lovelace Brain Mapping center for organizing and supervising the *in vivo* MRI studies. The authors would also like to thank Dr. Fishbein and the Translational Pathology Core Laboratory at UCLA for their histology services.

This work is supported by the National Eye Institute (NEI) Grant# R01EY021590 and the National Institute of Biomedical Imaging and Bioengineering (NIB IB) Grant# R21EB015084 and Grant# R21EB016896.

Manuscript received September, 2016. This work was supported in part by the National Institute of Biomedical Imaging and Bioengineering (NIBIB) Grant# R21EB015084 and Grant# R21EB016896.

Biography

Neha Bajwa received the B.S. degree in biomedical engineering from The Johns Hopkins University, Baltimore, MD, USA, with a concentration in cell tissue engineering, in 2008, and M.S. and Ph.D. degrees in biomedical engineering from the University of California, Los Angeles (UCLA), CA, USA, in 2010 and 2016, respectively. She has focused her research on THz imaging for diagnostic applications (i.e. tissue viability assessment) in burn and flap wound models. Additionally, she is investigating THz imaging contrast using companion MRI.

Shijun Sung received the B.S. degrees in electrical engineering at University of California, Los Angeles (UCLA), CA, USA, in 2011, and is currently a graduate student in the Department of Electrical Engineering and performs research with a number of faculty members and researchers in the Department of Bioengineering and in the David Geffen school of medicine. His research interests include THz medical imaging, THz optical and quasi-optical design, THz system design, and corneal water content sensing.

Daniel Ennis received the PhD degree from Johns Hopkins University in 2004, and trained as a Post-doctoral fellow at Stanford University from 2004–2006. He is currently an associate professor in the Departments of Radiological Sciences and Bioengineering. Professor Ennis is interested in both the basic science and clinical applications of MRI for evaluating cardiovascular structure, function, and remodeling. In particular, his group is currently focused on developing advanced methods for pediatric cardiovascular exams that may improve patient acceptance, while maintaining or improving diagnostic image quality.

Michael Fishbein received the M.D. degree from the University of Illinois College of Medicine at Chicago in 1971, and trained in Anatomic and Clinical Pathology at the Harbor University of California Los Angeles Medical center from 1972–1975. He is a Professor of Pathology and Laboratory Medicine at UCLA, Los Angeles. He is also a Professor of Medicine at UCLA. He is Chief of Autopsy, Cardiovascular and Pulmonary Pathology as well as a Member of the JCCC Thoracic Oncology Program. His current research interests include Autopsy, Cardiovascular and Pulmonary Pathology, and Surgical Pathology.

Bryan N. Nowroozi received the Ph.D. degree in ecology and evolutionary biology from Brown University, Providence, RI, USA, in 2011. He was a postdoctoral researcher in the UCLA Department of Bioengineering and the assistant director of graduate education at the UCLA Center for Advanced Surgical and Interventional Technology. His research interests are in medical imaging, haptic feedback, and biomechanics. He currently with Mimeo Labs Inc., Santa Monica, CA, USA.

Dan Ruan received her PhD degree from the University of Michigan, Ann Arbor, in 2008. She is currently an assistant professor in the Department of Radiation Oncology at UCLA. Dr. Ruan's research interests includes medical imaging, tomography, parametric and nonparametric estimation, dynamic systems, and general inverse problems in medical signal processing. Her current works focus on physics system modeling and characterization, algorithm development and performance analysis, as well as software-hardware system integration and validation. She is particularly interested in understanding the mathematics and physics in diagnostic radiology and radiation oncology.

Jeffry Alger received a PhD degree in biophysical chemistry under the direction of Professor James H. Prestegard at Yale University in 1979 and performed his postdoctoral training on multinuclear resonance magnetization transfer in the Yale Department of Molecular Biophysics and Biochemistry between 1979 and 1984. He was an assistant professor in the Yale Department of Radiology from 1984–1986. In 1994, Dr. Alger moved to Los Angeles and became a faculty member at the University of California, Los Angeles (UCLA) in the Department of Radiology and in the Ahmanson-Lovelace Brain Mapping Center. He was promoted to the rank of Professor in July 2000. His primary faculty appointment moved to the UCLA Department of Neurology in 2005. His current research lies in neuroscience imaging applications of MRI with focus on MRS, diffusion tensor imaging and perfusion imaging.

Ashkan Maccabi received the B.S. degrees in electrical engineering at University of California (UCLA), Los Angeles, CA, USA, in 2012, and is currently a graduate student in the Department of Electrical Engineering and performs research with a number of faculty members and researchers in the Department of Bioengineering and in the David Geffen school of medicine. His research interests included vibro-acoustography imaging, system design, and medical imaging.

Maie. A. St John received the M.D. degree and Ph.D degree from the School of Medicine at Yale University, New Haven, CT, in 1999, and trained in Surgery and Otolaryngology at the UCLA School of Medicine from 2001–2005. She is an Associate Professor-in-Residence in the Department of Head and Neck Surgery at UCLA. She has been named the Samuel and Della Perlman Chair in the Head and Neck Surgery Department, UCLA, an is Co-Director of the Head and Neck Cancer Program. She holds professional memberships in the American Academy of Otolarynology-Head and Neck Surgery, the American Head and Neck Society, the Triological Society, the American Association for Cancer Research, and the Los Angeles Biomedical Research Institute, to name a few. Her interests include understanding the mechanisms of tumor progression and metastasis in head and neck cancer and involving laboratory-based research for the development of novel therapies for head and neck cancer patients.

Warren S. Grundfest received the M.D. degree from the College of Physicians & Surgeons, Columbia University, New York, NY, USA, in 1980, and trained in General Surgery at University of California (UCLA), Los Angeles, CA, USA, and Cedars-Sinai Medical Center, Los Angeles, CA, USA, in 1985. He is a Professor of Bioengineering at the University of California (UCLA), Los Angeles, CA, USA. He is also a Professor of Electrical Engineering and Professor of Surgery at UCLA. His current research interests include excimer lasers for medical applications, optical diagnostic procedures, minimally invasive surgical tools, haptic feedback and ultrasound imaging. Dr. Grundfest was elected Fellow, American Institute of Medical & Biologic Engineers (AIMBE), for pioneering development and dissemination of minimally invasive surgery in 1996. In the same year, he was elected Fellow, Society of Photo-Optical Instrumentation Engineers (SPIE), for his distinguished & valuable contributions to the field of optical engineering in medicine & biology

Zachary D. Taylor (S'06-M'09) received the B.S. degree in electrical engineering from the University of California (UCLA), Los Angeles, CA, USA, in 2004, and the M.S. and Ph.D. degrees in electrical engineering from the University of California (UCSB), Santa Barbara, CA, USA, in 2006 and 2009, respectively. He is an adjunct assistant professor with the University of California (UCLA), Los Angeles, CA, USA, with appointments in the Department of Bioengineering, Department of Surgery, and Department of Head and Neck Surgery. He is currently conducting biomedical THz imaging research in collaboration with the departments of Neurosurgery, Neuropathology, Pathology, General surgery, and Ophthalmology at the UCLA David Geffen School of Medicine. Additionally, he is working on THz system design, THz optics design, and image processing techniques to improve THz image acquisition rates.

References

[1]. Epstein FH and McCord JM, "Oxygen-Derived Free Radicals in Postischemic Tissue Injury," N. Engl. J. Med, vol. 312, no. 3, pp. 159–163, 1 1985. [PubMed: 2981404]

[2]. DiBona DR and Powell WJ, "Quantitative correlation between cell swelling and necrosis in myocardial ischemia in dogs.," Circ. Res, vol. 47, no. 5, pp. 653–665, 1980. [PubMed: 7418125]

[3]. Drager LF, Abe JM, Martins MA, Lotufo PA, and Bensenor IJM, "Impact of clinical experience on quantification of clinical signs at physical examination," J. Intern. Med, vol. 254, no. 3, pp. 257–263, 9 2003. [PubMed: 12930235]

[4]. Gerber LH, "A review of measures of lymphedema," Cancer, vol. 83, no. S12B, pp. 2803–2804, 12 1998. [PubMed: 9874401]

[5]. Siegel PH, "Terahertz technology in biology and medicine," in Microwave Symposium Digest, 2004 IEEE MTT-S International, 2004, vol. 3, p. 1575–1578 Vol.3.

[6]. Taylor ZD et al., "THz medical imaging: in vivo hydration sensing," Terahertz Sci. Technol. IEEE Trans. On, vol. 1, no. 1, pp. 201–219, 2011.

[7]. Woodward RM et al., "Terahertz pulse imaging in reflection geometry of human skin cancer and skin tissue," Phys. Med. Biol, vol. 47, no. 21, p. 3853, 2002. [PubMed: 12452577]

[8]. Sung S et al., "Fast-scanning THz medical imaging system for clinical application," Proc SPIE, 2012, vol. 8496, p. 84960S–84960S-7.

[9]. Taylor ZD et al., "THz and mm-Wave Sensing of Corneal Tissue Water Content: Electromagnetic Modeling and Analysis," IEEE Trans. TerahertzSci. Technol, vol. 5, no. 2, pp. 170–183, 3 2015.

[10]. Tewari P et al., "In vivo terahertz imaging of rat skin burns," J. Biomed. Opt, vol. 17, no. 4, pp. 0405031–0405033, 2012.

[11]. Taylor ZD et al., "Active THz medical imaging using broadband direct detection," Proc SPIE, 2013, vol. 8624, pp. 862403–862403–10.

[12]. Hu BB and Nuss MC, "Imaging with terahertz waves," Opt. Lett, vol. 20, no. 16, p. 1716, 8 1995. [PubMed: 19862134]

[13]. Jin Y-S, Kim G-J, and Jeon S-G, "Terahertz dielectric properties of polymers," J. KoreanPhys. Soc, vol. 49, no. 2, pp. 513–517, 2006.

[14]. Fitzgerald AJ, Berry E, Zinovev NN, Walker GC, Smith MA, and Chamberlain JM, "An introduction to medical imaging with coherent terahertz frequency radiation," Phys. Med. Biol, vol. 47, no. 7, p. R67, 2002. [PubMed: 11996068]

[15]. Pickwell E, Cole BE, Fitzgerald AJ, Pepper M, and Wallace VP, “In vivo study of human skin using pulsed terahertz radiation,” Phys. Med. Biol, vol. 49, no. 9, p. 1595, 2004. [PubMed: 15152918]

[16]. Bajwa N et al., “Reflective THz and MR imaging of burn wounds: a potential clinical validation of THz contrast mechanisms,” Proc SPIE, 2012, vol. 8496, p. 84960X–84960X-7.

[17]. Wallace VP et al., “Terahertz pulsed spectroscopy of human basal cell carcinoma,” Appl. Spectrosc, vol. 60, no. 10, pp. 1127–1133, 2006. [PubMed: 17059664]

[18]. Ablett S, Carpenter TA, Hall LD, Hodgson RJ, and Salter DC, “MRI microscopy of human skin,” in Soc. Magn. Reson. Med 10th Annual Scientific Meeting, 1991, p. 1251.

[19]. Mirrashed F and Sharp JC, “In vivo morphological characterisation of skin by MRI micro-imaging methods,” Skin Res. Technol, vol. 10, no. 3, pp. 149–160, 2004. [PubMed: 15225264]

[20]. Richard S et al., “In Vivo Proton Relaxation Times Analysis of the Skin Layers by Magnetic Resonance Imaging,” J. Invest. Dermatol, vol. 97, no. 1, pp. 120–125, 7 1991. [PubMed: 2056181]

[21]. Budinger TF and Lauterbur PC, “Nuclear magnetic resonance technology for medical studies,” Science, vol. 226, no. 4672, pp. 288–298, 10 1984. [PubMed: 6385252]

[22]. Richard S et al., “Characterization of the Skin In Vivo by High Resolution Magnetic Resonance Imaging: Water Behavior and Age-Related Effects,” J. Invest. Dermatol, vol. 100, no. 5, pp. 705–709, 5 1993. [PubMed: 8388010]

[23]. Khoury NJ, El-Khoury GY, and Kathol MH, “MRI diagnosis of diabetic muscle infarction: report of two cases,” Skeletal Radiol., vol. 26, no. 2, pp. 122–127, 2 1997. [PubMed: 9060105]

[24]. Baxter CR, “Fluid volume and electrolyte changes of the early postburn period,” Clin. Plast. Surg, vol. 1, no. 4, pp. 693–703, 10 1974. [PubMed: 4609676]

[25]. Demling RH, “The burn edema process: current concepts,” J. Burn Care Res, vol. 26, no. 3, pp. 207–227, 2005.

[26]. Demling RH, “Burn Edema. Part I: Pathogenesis. [Review],” J. Burn Care, vol. 3, no. 3, pp. 138–149, 6 1982.

[27]. Leape LL, “Early burn wound changes,” J. Pediatr. Surg, vol. 3, no. 2, pp. 292–299, 4 1968. [PubMed: 5659203]

[28]. Boykin JV, Eriksson E, and Pittman RN, “Microcirculation of a scald burn: an in vivo experimental study of the hairless mouse ear,” Burns, vol. 7, no. 5, pp. 335–338, 1981.

[29]. Brouhard BH, Carvajal HF, and Linares HA, “Burn edema and protein leakage in the rat: I. Relationship to time of injury,” Microvasc. Res, vol. 15, no. 2, pp. 221–228, 1978. [PubMed: 661613]

[30]. DEMLING RH, MAZESS RB, and WOLBERG W, “The effect of immediate and delayed cold immersion on burn edema formation and resorption.,” J. Trauma Acute Care Surg, vol. 19, no. 1, pp. 56–60, 1979.

[31]. Chu C-S, Matylevich NP, McManus AT, Mason AD, and Pruitt BA, “Direct current reduces wound edema after full-thickness burn injury in rats,” J. Trauma Acute Care Surg, vol. 40, no. 5, pp. 738–742, 1996.

[32]. Dorsett-Martin WA, “Rat models of skin wound healing: A review,” Wound Repair Regen, vol. 12, no. 6, pp. 591–599, 11 2004. [PubMed: 15555049]

[33]. Heimbach D, Engrav L, Grube B, and Marvin J, “Burn depth: a review,” World J. Surg, vol. 16, no. 1, pp. 10–15, 1992. [PubMed: 1290249]

[34]. Hargroder AG, Davidson JE Sr, Luther DG, and Head JF, “Infrared imaging of burn wounds to determine burn depth,” in AeroSense’99, 1999, pp. 103–108.

[35]. Arbab MH, Winebrenner DP, Dickey TC, Chen A, Klein MB, and Mourad PD, “Terahertz spectroscopy for the assessment of burn injuries in vivo,” J. Biomed. Opt, vol. 18, no. 7, pp. 77004–77004, 2013.

[36]. Wang JF, Olson ME, Reno CR, Kulyk W, Wright JB, and Hart DA, “Molecular and Cell Biology of Skin Wound Healing in a Pig Model,” Connect. Tissue Res, vol. 41, no. 3, pp. 195–211, 1 2000. [PubMed: 11264869]

[37]. Taylor ZD et al., "THz medical imaging: in vivo hydration sensing," Terahertz Sci. Technol. IEEE Trans. On, vol. 1, no. 1, pp. 201–219, 2011.

[38]. Taylor ZD et al., "THz and mm-Wave Sensing of Corneal Tissue Water Content: In Vivo Sensing and Imaging Results," Terahertz Sci. Technol. IEEE Trans. On, vol. 5, no. 2, pp. 184–196, 2015.

[39]. Di Sieno L et al., "Toward noninvasive assessment of flap viability with time-resolved diffuse optical tomography: a preclinical test on rats," J. Biomed. Opt, vol. 21, no. 2, pp. 025004–025004, 2016.

[40]. Joris I and Majno G, Cells, tissues, and disease: principles of general pathology. Oxford University Press, USA, 2004.

[41]. Koruda MJ et al., "Assessing burn wound depth using in vitro nuclear magnetic resonance (NMR)," J. Surg. Res, vol. 40, no. 5, pp. 475–481, 5 1986. [PubMed: 3736031]

[42]. Cameron IL, Ord VA, and Fullerton GD, "Characterization of proton NMR relaxation times in normal and pathological tissues by correlation with other tissue parameters," Magn. Reson. Imaging, vol. 2, no. 2, pp. 97–106, 1 1984. [PubMed: 6530924]

[43]. Brans TA, Dutrieux RP, Hoekstra MJ, Kreis RW, and Du Pont JS, "Histopathological evaluation of scalds and contact burns in the pig model," Burns, vol. 20, pp. S48–S51, 1994. [PubMed: 8198744]

[44]. Bajwa N, Sung S, Fishbein M, Grundfest WS, and Taylor ZD, "Exploration of the effects of burn parameters on THz wound imaging," Proc SPIE, 2015, vol. 9585, p. 95850T–95850T-6.

[45]. Granger HJ, "Role of the interstitial matrix and lymphatic pump in regulation of transcapillary fluid balance," Microvasc. Res, vol. 18, no. 2,pp. 209–216, 1979. [PubMed: 386049]

[46]. Lund T, Onarheim H, and Reed RK, "Pathogenesis of edema formation in burn injuries," World J. Surg, vol. 16, no. 1, pp. 2–9, 1 1992. [PubMed: 1290261]

[47]. LEAPE LL, "Initial changes in burns: tissue changes in burned and unburned skin of rhesus monkeys.," J. Trauma Acute Care Surg, vol. 10, no. 6, pp. 488–492, 1970.

[48]. Onarheim H and Reed RK, "Thermal skin injury: effect of fluid therapy on the transcapillary colloid osmotic gradient," J. Surg. Res, vol. 50, no. 3,pp. 272–278, 1991. [PubMed: 1999916]

[49]. Sakurai H, Nozaki M, Traber LD, Hawkins HK, and Traber DL, "Microvascular changes in large flame burn wound in sheep," Burns, vol. 28, no. 1, pp. 3–9, 2002. [PubMed: 11834323]

[50]. Eberhart RC and Shitzer A, Heat Transfer in Medicine and Biology: Analysis and Applications. Springer Science & Business Media, 2012.

[51]. McGrath JA, Eady RAJ, and Pope FM, "Anatomy and organization of human skin," Rooks Textb. Dermatol. Burns TB Cox NAl Eds, vol. 8, 2004.

[52]. Paul W and Sharma CP, Advances in Wound Healing Materials: Science and Skin Engineering. Smithers Rapra Technology, 2015.

[53]. Warner RR, Myers MC, and Taylor DA, "Electron probe analysis of human skin: determination of the water concentration profile," J. Invest. Dermatol, vol. 90, no. 2, pp. 218–224, 1988. [PubMed: 3339263]

[54]. Demling RH, Gunther RA, Harms B, and Kramer G, "Burn Edema Part II: Complications, Prevention, and Treatment.," J. Burn Care Res, vol. 3, no. 4, p. 799, 1982.

[55]. A. G, "Microvascular permeability to macromolecules in thermal injury.," Acta Physiol. Scand. Suppl, vol. 463, pp. 111–122, 12 1978.

[56]. Liebe HJ, Hufford GA, and Manabe T, "A model for the complex permittivity of water at frequencies below 1 THz," Int. J. Infrared Millim. Waves, vol. 12, no. 7, pp. 659–675, 1991.

[57]. Pickwell E, Cole BE, Fitzgerald AJ, Wallace VP, and Pepper M, "Simulation of terahertz pulse propagation in biological systems," Appl. Phys. Lett, vol. 84, no. 12, pp. 2190–2192, 2004.

[58]. Bennett DB, Li W, Taylor ZD, Grundfest WS, and Brown ER, "Stratified media model for terahertz reflectometry of the skin," IEEE Sens. J, vol. 11, no. 5, pp. 1253–1262, 2011.

[59]. Maccabi A et al., "Reflectivity measurements of water and dioxane mixtures using a 100 GHz Gunn diode source," 2013, vol. 8585, p. 85850X–85850X-7.

[60]. Sowa MG, Payette JR, and Mantsch HH, "Near-infrared spectroscopic assessment of tissue hydration following surgery," J. Surg. Res, vol. 86, no. 1, pp. 62–69, 1999. [PubMed: 10452870]

[61]. Brodovicz KG, McNaughton K, Uemura N, Meininger G, Girman CJ, and Yale SH, “Reliability and feasibility of methods to quantitatively assess peripheral edema,” Clin. Med. Res, vol. 7, no. 1–2, pp. 21–31, 2009. [PubMed: 19251582]

[62]. Notohamiprodjo M et al., “MR lymphangiography at 3.0 T: correlation with lymphoscintigraphy,” Radiology, vol. 264, no. 1, pp. 78–87, 2012. [PubMed: 22523325]

[63]. Mihara M et al., “Indocyanine green (ICG) lymphography is superior to lymphoscintigraphy for diagnostic imaging of early lymphedema of the upper limbs,” PloS One, vol. 7, no. 6, p. e38182, 2012. [PubMed: 22675520]

[64]. WARD PA and TILL GO, “Pathophysiologic events related to thermal injury of skin.,” J. Trauma Acute Care Surg, vol. 30, pp. 75–79, 1990.

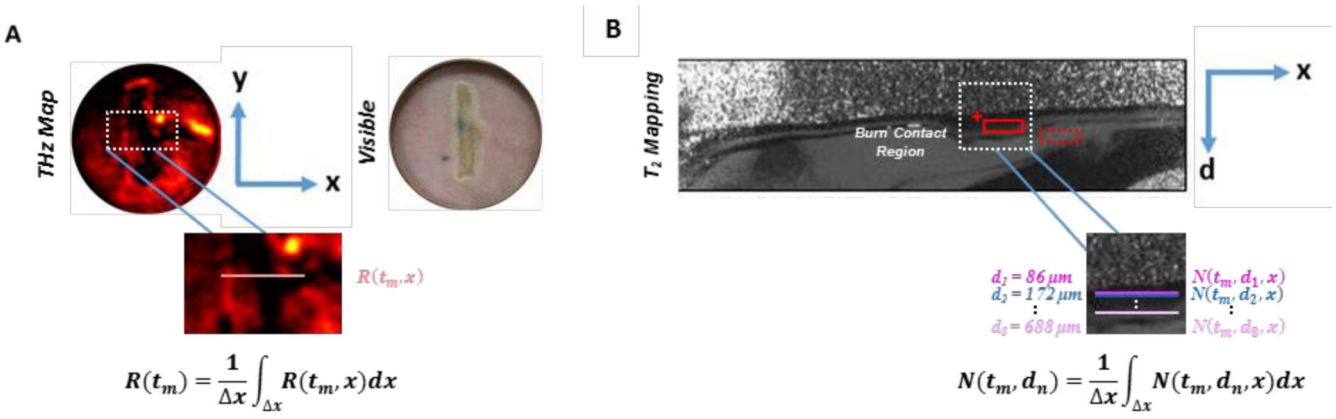

Figure 1:

Spatial dimensions and segmentation of (a) a THz image and (b) its companion MRI image for a full thickness burn at t=90 min. Both THz and MRI images are 2-dimensional. While THz images provide reflectivity measurements in the x and y dimensions, MRI images furnish TWC information in the x and depth (d) dimension. In the T_2w MRI scans, layers of the skin are clearly delineated where the outer bright thin line (red cursor) corresponds to the epidermis. The dermis (red solid rectangle) appears as a dark layer, while the hypodermis (red dotted rectangle) is bright. Dotted white rectangles denote the location of the burn contact region, which are magnified to show the burn segmentation methods used. For all time-series THz images, mean reflectivity is calculated for a single contour drawn along the x-dimension of the burn contact area. $R(t_m)$ represents the mean reflectivity at time t_m along length x of the contour. Mean relative proton density is calculated for multiple contours drawn along the x-dimension of the burn contact region at incrementally increasing depths (d_n) in the companion MRI image. $N(t_m, d_n)$ represents the mean relative proton density at time t_m and depth d_n along length x of the contour. This analysis represents a one-to-multiple relationship between THz and MRI data, respectively: At every time point, mean reflectivity across the burn region is compared to mean relative proton density for multiple depths of the burn tissue.

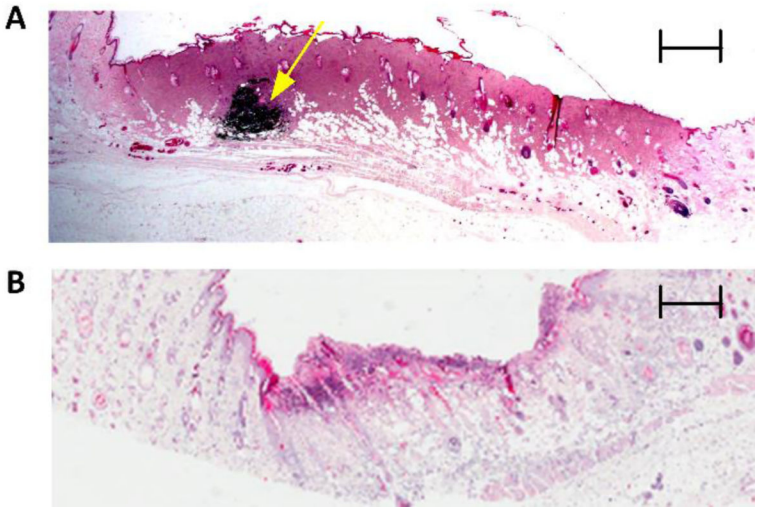

Figure 2:

Histological assessment of burn wound severity. Representative 2X hematoxylin and eosin (H&E) staining of a full thickness wound (A) and a partial thickness wound (B) 72 h post burn induction. Coagulation and red brick myocardial necrosis in the dermis and subcutaneous layers are used to classify (A) as full thickness. An intradermal fiducial marker (solid yellow arrow) is clearly visible. *Scale bar,* 800 μm. Revascularization of tissue as well as intact subcutaneous and muscle layers are used to confirm (B) as partial thickness. *Scale bar,* 600 μm.

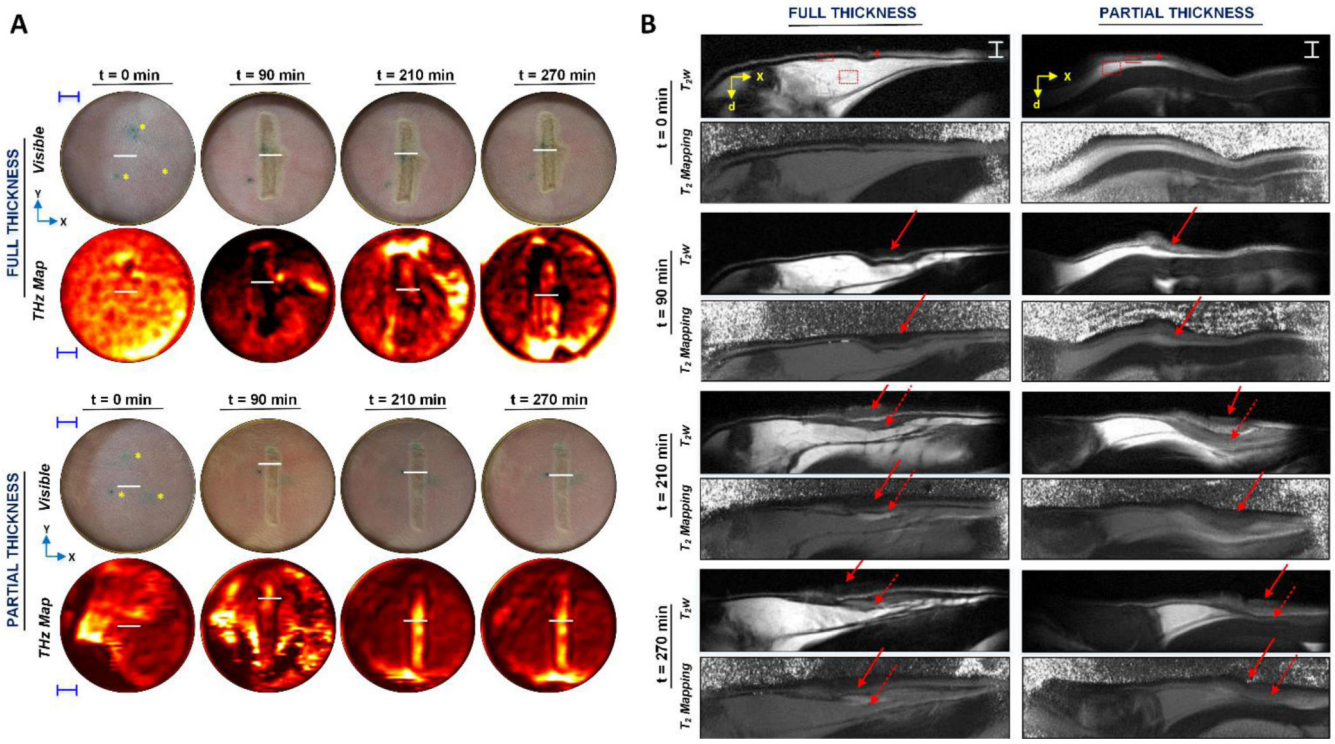

Figure 3:

Concomitant THz and MRI time-series imagery of burn wounds *in vivo.* (A) 2D THz and visible imagery of a rectangular partial thickness and full thickness wound prior to and following burn induction (t=90 min) in rat abdominal skin *in vivo.* THz image sets are displayed in a standard false color map where black-red-yellow-white denotes increasing normalized THz reflectivity. Yellow asterisks in the abdominal skin of visible images at t=0 min indicate intradermal fiducial tattoos. *Blue scale bars,* 5 mm. (B) Companion MRI imagery includes 2D transverse T_2w MRI scans and T_2-mapping. All MRI slices spatially map to white linear contours, indicated by solid white horizontal lines, shown in their respective THz and visible imagery. MRI images are displayed in a gray-scale color map where black-grey-white indicates increasing intensity and T_2 time for T_2w and T_2-mapping images, respectively. At t=0 min in the T_2w MRI scans, layers of the skin are clearly delineated where the outer bright thin line (red cursor) corresponds to the epidermis. The dermis (red solid rectangle) appears as a dark layer, while the hypodermis (red dotted rectangle) is bright. *White horizontal scale bars,* 1.9 mm. Localization of the burn and fluid ingress are demarcated by solid and dashed arrows, respectively. For both a, and b, “x,” “y,” and “d” in the axes denote the horizontal, vertical, and depth dimensions, respectively, of a rat imaged in supine position for the THz and visible images and in prone position for parallel MRI imagery. By t=210 and 270 min, MRI and THz signal, both of which appear brighter in a partial thickness wound, become spatially organized within the burn contact area of each wound.

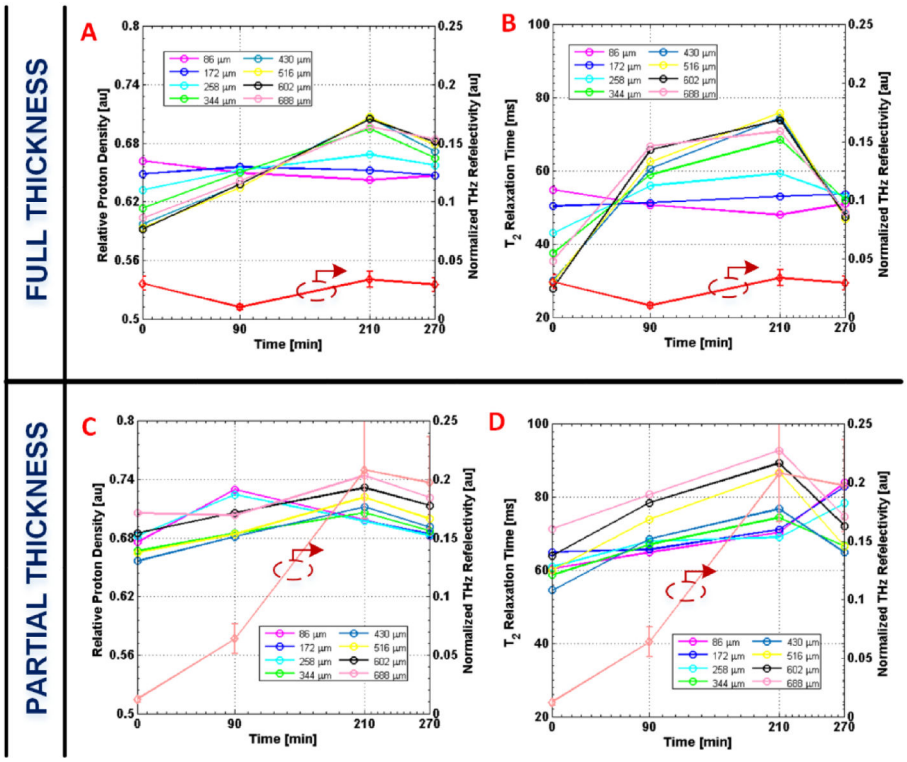

Figure 4:

Temporal plots of THz and depth-dependent MRI parameters. Plots comparing mean relative proton densities (i.e. mobile TWC or edema) and mean T_2 relaxation times at varying skin depths with normalized THz reflectivity as a function of time for a full thickness wound (A, B) and a partial thickness wound (C, D). Burns are induced at t=90 min. Normalized THz reflectivity is calculated from white horizontal line segments delineated in Fig. 1a. Mean MRI values are generated for similar contours that segment the same burn region at specific depths in the tissue (see Methods). All multi-colored depth traces correspond to the left axis of the y-y plots, while the red traces correspond to the right axis. *Error bars,* ± 1 standard deviation. THz reflectivity grows and declines in parallel with MRI measurements at greater depths (> 258 μm), and their biphasic pattern is consistent with fluid shifts previously reported for burn edema pathogenesis. As predicted, partial thickness wounds, which experience more dermal perfusion, reveal THz reflectivity and MRI values of greater magnitude compared to those of a full thickness wound.

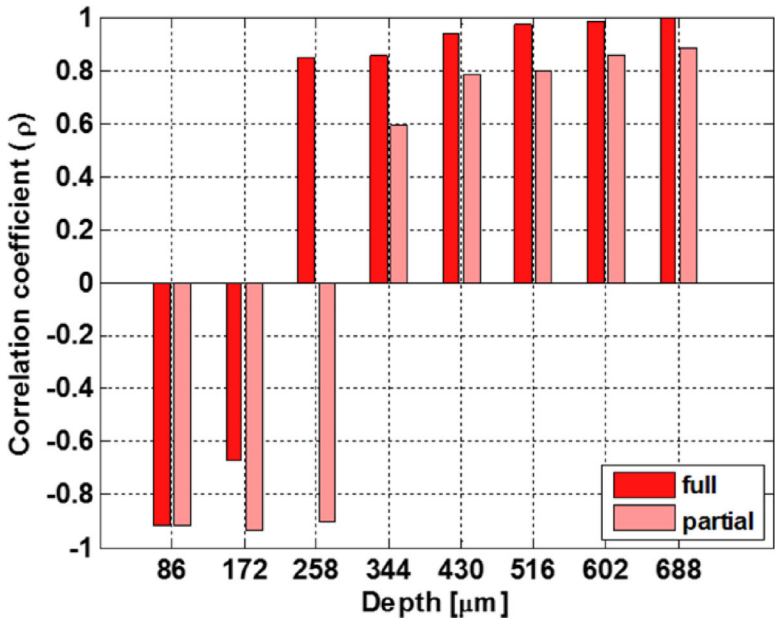

Figure 5:

Temporal correlations of THz and MRI as a function of depth. Temporal normalized cross-correlation coefficients were computed from THz reflectivity profiles and relative proton density profiles, which vary with depth, for both a partial thickness (pink) and full thickness (red) wound. THz reflectivity and MRI measurements of a full thickness wound at t=90 min was excluded. The horizontal axis corresponds to the variable d_n in the Methods section. The vertical axis corresponds to $p(d_n)$ in equation 6 of the Methods section. The most important result is that temporal correlations between THz and MRI imaging performed at greater depths (>258 μm) result in large, positive coefficients (p).It is within these deeper tissue layers of skin, specifically the dermis, that most changes in TWC following injury occur. Surface layers of the dermis display strongly negative behavior. The crossover point at ~ 258 μm is just beyond the dermoepidermal junction. The depth-dependent variation in the temporal correlation coefficients is also correlated between the wound severities. Results from both wound models suggest that mobile TWC strongly contributes to the overall observed THz contrast and that THz imaging tracks water movement at depths in tissue that may be useful for edema assessment.

TABLE 1:

Comparative analysis of TWC assessment techniques

TWC assessment method	Spatial TWC Map	Temporal TWC Map	Time of implementation following onset of injury	Measurement acquisition time (min)	References
Terahertz Imaging	Yes	Yes	Immediate	~10 min	[37]
MRI	Yes	Yes	Immediate	~40 – 60 min	[62]
Clinical inspection	No	No	Few hours	~5	[60], [63]
Water Displacement	No	Yes	~30 min	~20 – 30 min	[4]
Biopsy / Histology	Yes	No	Several hours	Few days	[61]

IEEE Trans Biomed Eng. Author manuscript; available in PMC 2019 June 20.